SLAC-PUB-3594
March 1985
(M)

ENERGY-DEPENDENCE OF INNER POTENTIAL IN Fe FROM LOW-ENERGY ELECTRON ABSORPTION (TARGET CURRENT)*

E. Tamura†, R. Feder‡, J. Krewer†, R. E. Kirby,
E. Kisker†, E. L. Garwin and F. K. King

Stanford Linear Accelerator Center
Stanford University, Stanford, California 94305

Abstract

For unpolarized low-energy electrons (0-60 eV) incident on a Fe(001) surface, the measured current I absorbed by the crystal (target current) displays a considerable amount of fine structure depending on the angle of incidence. Dynamical calculations of the elastic reflection coefficient R_e show that $-d^2R_e/dE^2$ is in good agreement with d^2I/dE^2 for suitably chosen real and imaginary parts of the inner potential. The energy dependence of the latter is thereby determined. Comparison with a bulk band structure calculated using the same real potential reveals a correspondence between target current minima and band gaps as well as current maxima and critical points.

Submitted to Solid State Communications

* Work supported by the Department of Energy, contract DE-AC03-76SF00515.

† Permanent address: Institut für Festkörperforschung, KFA Jülich, Postfach 1913, D-5170 Jülich, W. Germany

‡ Permanent address: Theoretische Festkörperphysik, FB 10, Universität Duisburg GH, D-4100 Duisburg, W. Germany

1. Introduction

Characteristic aspects of the electronic structure of solids and their surfaces at energies above the vacuum level, like the energy dependence of the bulk inner potential and surface scattering resonances, are most directly revealed by electron spectroscopic methods, which involve only one half-space state (like elastic Low-Energy Electron Diffraction (LEED)) (cf. e.g. [1-3] and refs. therein) or permit the isolation of a single state by eliminating a comparatively smooth background, like measuring the total elastic plus inelastic reflection coefficient, secondary electron emission (cf. [4,5] and refs. therein) or the current absorbed by the crystal (target current) (cf. [3,6-8] and refs. therein). By virtue of complementarity and time reversal, the information content of these 'single-state' methods is basically the same, the single state always being the LEED state of the semi-infinite system. From the experimental side, however, it is certainly the target current that is most easily accessible.

In view of the topical interest in 3d-metal ferromagnetism and its study by photoemission and bremsstrahlung (cf. [9-13] and refs. therein) we have investigated both experimentally and theoretically the target current for Fe(001), with the chief aims (a) of determining the energy dependence of the inner potential for states above the vacuum energy and (b) of identifying manifestations of the quasi-particle bulk band structure. In Sections 2 and 3 special features of our experimental and theoretical methods are outlined. Results are presented and discussed in Section 4.

2. Experiment

The experimental ultrahigh-vacuum set-up has been described elsewhere [20]. The sample was a demagnetized thin disk of Fe(100), cleaned in situ by repeated ion etching and heating cycles. The energy width of the electron beam was about 0.3 eV, the angular width about $+/-6^{o}$. Care was taken to ensure that the observed fine structures in the absorbed current function are not caused by spurious effects.

3. Theory

For an electron current of unit intensity, kinetic energy E and spin polarization σ (with σ=+/- refering to spin alignment parallel/antiparallel to the majority spin direction of the crystal) incident at polar angle θ in the azimuth ϕ, the current absorbed by the crystal (target current) is complementary to the entire back-scattered current, i.e.

$$I_{\sigma}(E,\theta,\phi) = 1 - R_{e\sigma}(E,\theta,\phi) - R_{i\sigma}(E,\theta,\phi) \quad , \qquad (1)$$

where R_e and R_i are the elastic and inelastic reflection coefficients, respectively. R_e is the sum of the intensities of the LEED beams, which emerge from the crystal for E,θ and ϕ, and can therefore be calculated accurately by dynamical LEED theory [1,2]. R_i comprises all the electrons leaving the crystal at energies E'<E and arbitrary angles. These integrations, while rendering its calculation very complicated, have the effect that R_i as a function of energy and angles varies only slowly compared to R_e. Contact with the experimental target current can therefore be made

by taking, for fixed θ and ϕ, the second energy derivative of eq.(1): $I''_\sigma = -R''_{e\sigma}$. (The second derivative is preferable to the first, as it eliminates not only a constant "background" but also a linearly rising one).

For the exchange-induced scattering asymmetry $A = (I_+ - I_-)/(I_+ + I_-)$ we note that in the case of features, which vary weakly over the range of the exchange splitting $\Delta E(E)$, A can be approximated in first order as

$$A(E) = \Delta E(E)/(2I(E)), \text{ with } I = (I_+ + I_-)/2 \quad . \tag{2}$$

This means that A can be estimated already from spin-averaged data (i.e. using unpolarized electrons), and that even without knowing the values of ΔE the zero crossings and signs of A are determined. For spin-polarized experiments this provides a useful consistency check. It is important to note that the inelastic reflection coefficient $R_{i\sigma}$ is still contained in the basic definition of A (cf. eq.(1)). To make contact with purely elastic calculations, a more suitable quantity is an asymmetry between second derivatives:

$$\tilde{A} := (I''_+ - I''_-)/(I''_+ + I''_-) \approx (R''_{e+} - R''_{e-})/(R''_{e+} + R''_{e-}) \quad . \tag{3}$$

In the present calculations of $R_{e\sigma}$ for Fe(001) we used the same real part of the muffin tin potential as in a previous magnetic (SP)LEED analysis for Fe(110) [14]. In particular, the spherically symmetric part (which contains the dominant spin dependence) was constructed with an energy-dependent local exchange approximation, and the real part of the uniform inner potential was $V_r(E) = 14.5 \exp(-E/E_0)$ (eV) with $E_0 = 350.9$ eV. For the imaginary part of the inner potential $V_i(E)$ we employed, in addition to the form

$0.85\ E^{1/3}$ from [14], various trial forms with the aim of determining the actual one via comparison with experiment. We note that the (SP)LEED study [14] does not cover the energy range between 0 and about 30 eV, in which the onset of plasmon-like excitations causes a strong rise in V_i. (in principle, V_r should also be varied, but the above form turned already out to be adequate). For the surface magnetization we took the bulk value, since its enhancement would only affect the asymmetry A, which is presently not available experimentally. For the one-dimensional surface potential barrier we used a truncated image model as well as a more sophisticated form proposed recently by Jones et al. [15]. In addition to the elastic reflection coefficient, we calculated for the same real (bulk) potential the corresponding bulk band structure in view of identifying one-dimensional bulk density of states features in the spectra.

The second energy derivatives of the calculated spin-averaged R_e and of the experimental target current were both obtained by means of a cubic spline fit routine [16]. To retrieve maximal physical information from given data, the smoothing (characterized by the spline fit parameter δy, the allowed deviation from the actual value) should be minimal with the constraint that statistical fluctuations are eliminated. For the present experimental data, we thus found $\delta y=0.001$ for every point. For the theoretical results, the uncertainty due to computer accuracy would allow a far weaker amount of smoothing. To compare with experiment, we found it however more appropriate to take a somewhat larger smoothing than for the experimental data, since these already contain a smoothing due to energy and angular broadening. This eliminates the theoretical LEED 'fine structure' (over energy intervals 0.5 eV), e.g. Rydberg resonances associated with beam emergence thresholds.

4. Results

Experimental and theoretical spectra are shown in Figures 1 and 2 for unpolarized electrons incident normally and 20^0 off-normal (in the (010) azimuth) respectively, on an Fe(001) surface. The measured target current I(E) (normalized to the primary current) is seen to reach its maximun close to 1 within 0.3 eV from threshold, corresponding to the energy width of the electron beam. It then decreases smoothly and crosses through zero (not shown) at about 110 eV. This decrease is plausible since with increasing energy the escape cone for inelastically scattered electrons widens and the true secondary yield increases. This interpretation is corroborated by the absence of such a decrease in the calculated purely elastic spectra $1-R_e(E)$ (cf. panel b in Figs. 1 and 2).

The small structures in I(E) and $1-R_e(E)$ are strongly enhanced in the second derivatives, with minima in the latter corresponding to maxima in the original spectra. (The steep rise of I near 0 eV was disregarded in calculating I", since it merely reflects the experimental energy spread). Features in the experimental I" and the calculated $-R_e''$ curves are seen to agree closely with each other in position, sign and size for both $\theta=0$ (Fig. 1) and $\theta=20^0$(Fig. 2). This explicitly confirms our assumption that inelastic processes did generally not produce significant structures. The agreement in positions of the features indicates that our choice of V_r (cf. also Fig. 3a) is appropriate. The decrease of the magnitude of the second-derivative features with increasing energy is due to an increasing broadening of the original structures by absorption out of the elastic channel, which is described by the imaginary potential V_{im}. Fig. 3b shows, in addition to the $E^{1/3}$ form, two other shapes of V_{im}, which we used in our calculations. The $-R_e''$ results obtained for these two shapes are compared in Fig. 1b and Fig. 2b. Above

20 eV, both are compatible with experiment, with a slight preference for the full-line V_{im}. In the energy range below 20 eV the normal-incidence data permit no distinction, while those for $\theta=20^{o}$ appear to favour again the full-line V_{im}. The observation that at $\theta=0^{o}$ (Fig. 1b) feature B is significantly larger in theory for both forms of V_{im} than in experiment suggest however that some other mechanism plays a role. Calculations for different angles of incidence θ reveal a shift of B, which is sufficient for angular averaging over the experimental $\pm 6^{o}$ divergence to broaden B in I and consequently reduce its height in I". This effect makes the smaller V_{im} acceptable also for $\theta=20^{o}$ around 12 eV. As for feature A for $\theta=20^{o}$, the twin minima obtained for the smaller V_{im} tend to merge by angular averaging and thus agree with experiment. In summary, the V_{im} given by the dashed line Fig. 3b is, with an estimated uncertainty of $\pm$ 0.1 eV, best below 20 eV. We note the good agreement with the values 0.8 eV and 0.7 eV reported for Ni at kinetic energy 2 eV in [17] and [18]. Also, it is consistent with the upper-state imaginary potential assumed in a recent bremsstrahlung study on Fe [12]. Differences in the R_e spectra obtained for different surface barriers were overridden by the smoothing chosen in the spline fit (cf. above).

The physical origin of the dominant features labelled A, B and C in Figures 1 and 2, which correspond to maxima in the target current, is revealed by the bulk band structure. For $\theta=0$, they are seen to occur at energies displaced from the critical points at H by about 1 eV towards the interior of the first three bands. For $\theta=20^{o}$, the additional band with its bottom ab about 4 eV gives rise to a minimum next to A in the -R"(E) curve for the weaker V_{im}. The shift of the target current maxima away from the maxima in the one-dimensional density of states is plausible, since the group velocity vanishes right at these maxima. This correlation has recently also been found

in angle-resolved secondary electron emission from Cu(001) [4,5]. A second type of correlation, which is well known from LEED [1], exist for the maxima of the second derivative, i.e. the target current mimima and elastic reflection coefficient maxima. The existence of a band gap is a sufficient but not necessary condition for these features (cf. the regions around 8, 36 and 50 eV in Fig. 1). If there is more than one k_z value at a given energy, the wave function inside the crystal contains a superposition of several propagating Bloch waves, and the resulting target current depends on their relative amplitudes. In view of the multitude of even-symmetry bands for off-normal incidence (cf. Fig. 2), the target current minima can therefore no longer be plausibly correlated with the band structure. LEED beam emergence thresholds (indicated by vertical arrows in Fig. 1 and 2) manifest themselves only as comparatively weak modulations.

The calculated exchange-induced elastic scattering asymmetry for spin-up and spin-down electrons is seen in Fig. 4 to reach maxima up to 8 % below 15 eV. The approximation according to eq.(2) (using $R_{e\sigma}$ instead of I_σ) is a semi-quantitative one.

5. Conclusion

For normal and off-normal angles of incidence of unpolarized electrons on Fe(001), the second energy derivative of the measured target current has been shown to agree well with the negative of the second derivative of the elastic reflection coefficient calculated by dynamical LEED theory. From this agreement, the energy dependence of the real and imaginary parts of the inner potential is found to be the same as in earlier LEED work above 30 eV.

It has also been determined (cf. Fig. 3a and dashed line in Fig. 3b) in the range 0-30 eV, which is particularly important for photoemission and its inverse (cf. [9-13]). Maxima of the target current are related to critical points in the bulk band structure, with a shift by about 1 eV into the respective band. Some minima correspond to band gaps, exspecially for normal incidence, i.e. along a high-symmetry direction.

Our results demonstrate the usefulness of target current spectroscopy in conjunction with dynamical LEED calculations and recommend an analogous study using polarized electrons [19]. In particular, this should shed more light on the spin-dependence of the imaginary potential (i.e. the inelastic mean free path) and on the exchange splitting of bulk energy bands above the vacuum level.

Acknowledgement

The experimental part of this work was supported by the Department of energy (contract DE-AC03-76SF00515), and the theoretical part by the Deutsche Forschungsgemeinschaft.

19) Experimentally, a spin dependence of the target current has already been observed on a metglass (H.C. Siegmann, D.T. Pierce and R.J. Celotta, Phys. Rev. Lett. 46, 452 (1981)) and on Fe(001) around 750 eV (L_2 threshold) (J. Kirschner, Sol. State Commun. 49, 39 (1984)).

20) E. Kisker, R.E. Kirby, E.L. Garwin, F.K. King, E. Tamura and R. Feder, J. Appl. Phys.

Figure Captions

Fig. 1: For electrons normally incident on Fe(001): (a) experimental normalized target current (– – –) and its second derivative (——); (b) theoretical spin-averaged $(1-R_e(E))$ (– – –) and $-R_e''(E)$ (——) calculated for the imaginary potential V_{im} given by full line in fig. 3b, and $-0.65\ R_e''(E)$ (····) for V_{im} given by dashed line in fig. 3b); vertical arrows indicate emergence thresholds of LEED beams; (c) bulk energy bands of Δ_1 symmetry for majority (——) and minority (– – –) spin electrons. (The energy is relative to the vacuum zero).

Fig. 2: As fig. 1, except incidence at polar angle $\theta=20^0$ in the (010) azimuth, and bulk bands of even symmetry with respect to plane of incidence.

Fig. 3: Inner potential versus incident energy: (a) real part $14.5 \exp(-E/350.9)$ (eV); (b) imaginary parts: $0.85\ E^{1/3}$ (····), linear (– – –) and intermediate (——) forms.

Fig. 4: Theoretical exchange-induced scattering asymmetry $A = (R_{e+} - R_{e+})/(R_{e+} + R_{e-})$ (——) and its approximation by eq.(2) with $\Delta E = 1.5$ eV and $R_{e\sigma}$ instead of I_σ (····), for polar angles $\theta=0^0$ and 20^0.

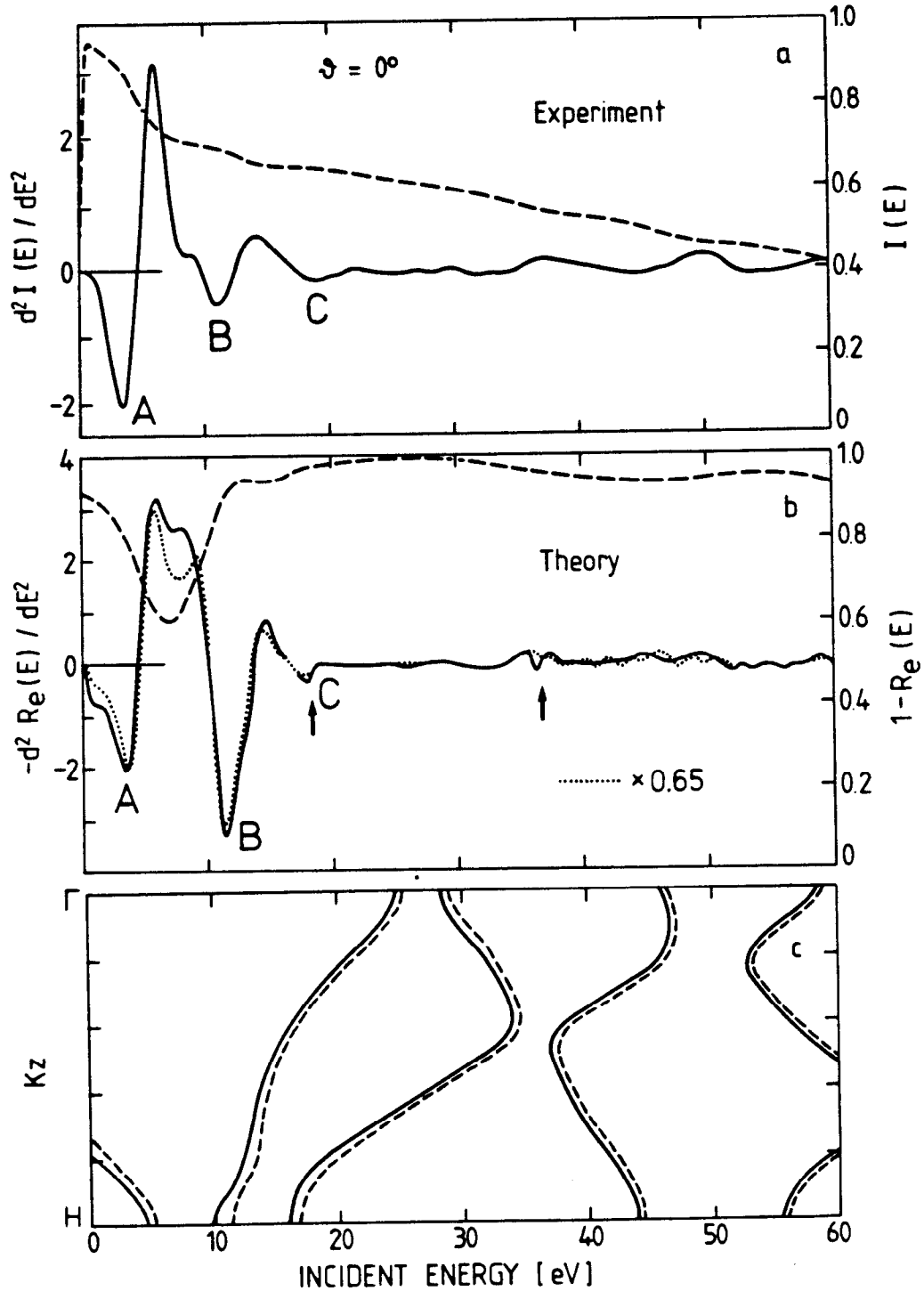
ϑ = 0°
a
Experiment
A
B
C
d² I (E) / dE²
I (E)
b
Theory
× 0.65
-d² Re(E) / dE²
1-Re (E)
c
Kz
Γ
H
INCIDENT ENERGY [eV]

Fig. 1

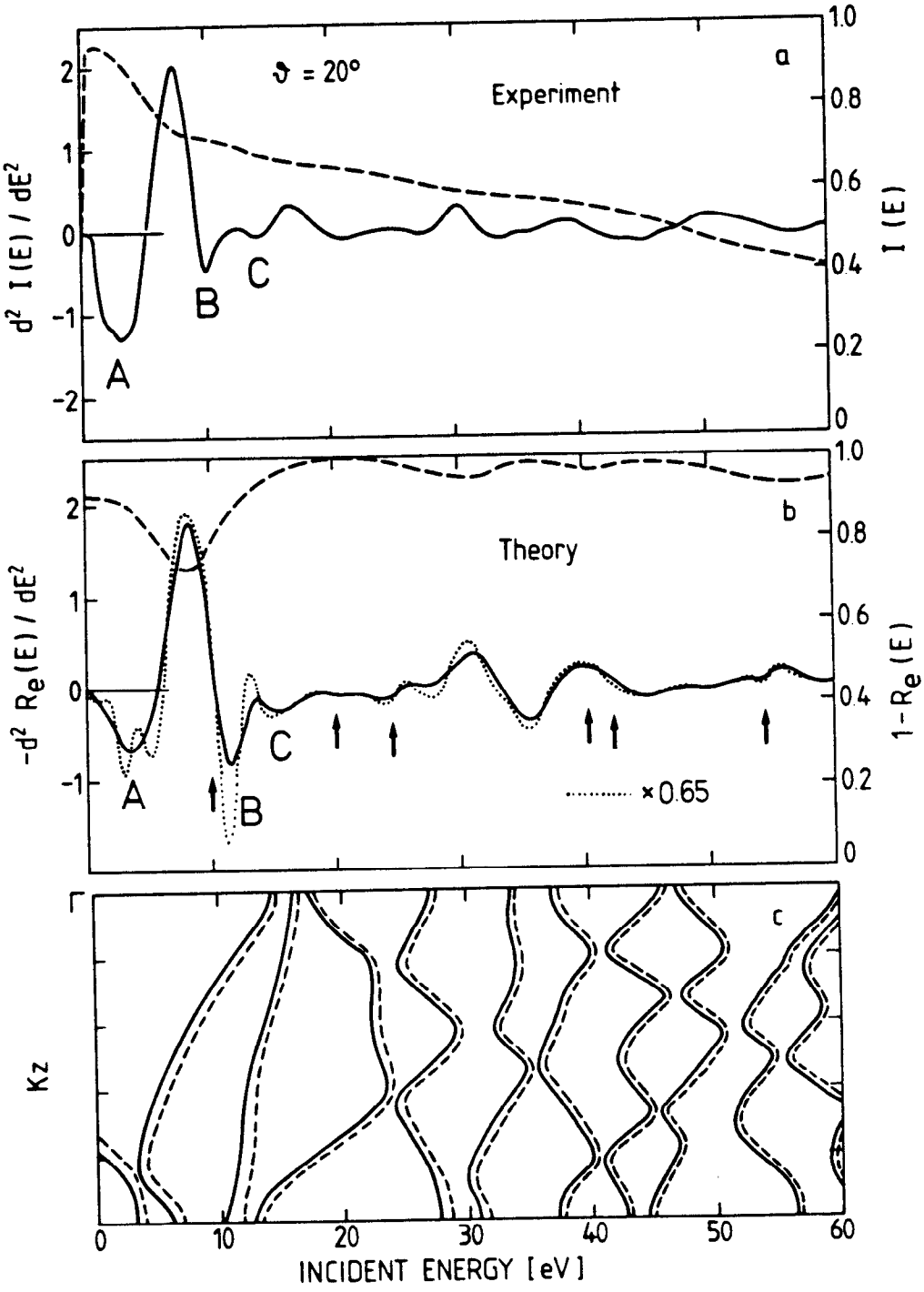
a
ϑ = 20°
Experiment
A
B
C
d² I(E) / dE²
I (E)
b
Theory
× 0.65
-d² Re(E) / dE²
1-Re(E)
c
Kz
INCIDENT ENERGY [eV]

Fig. 2

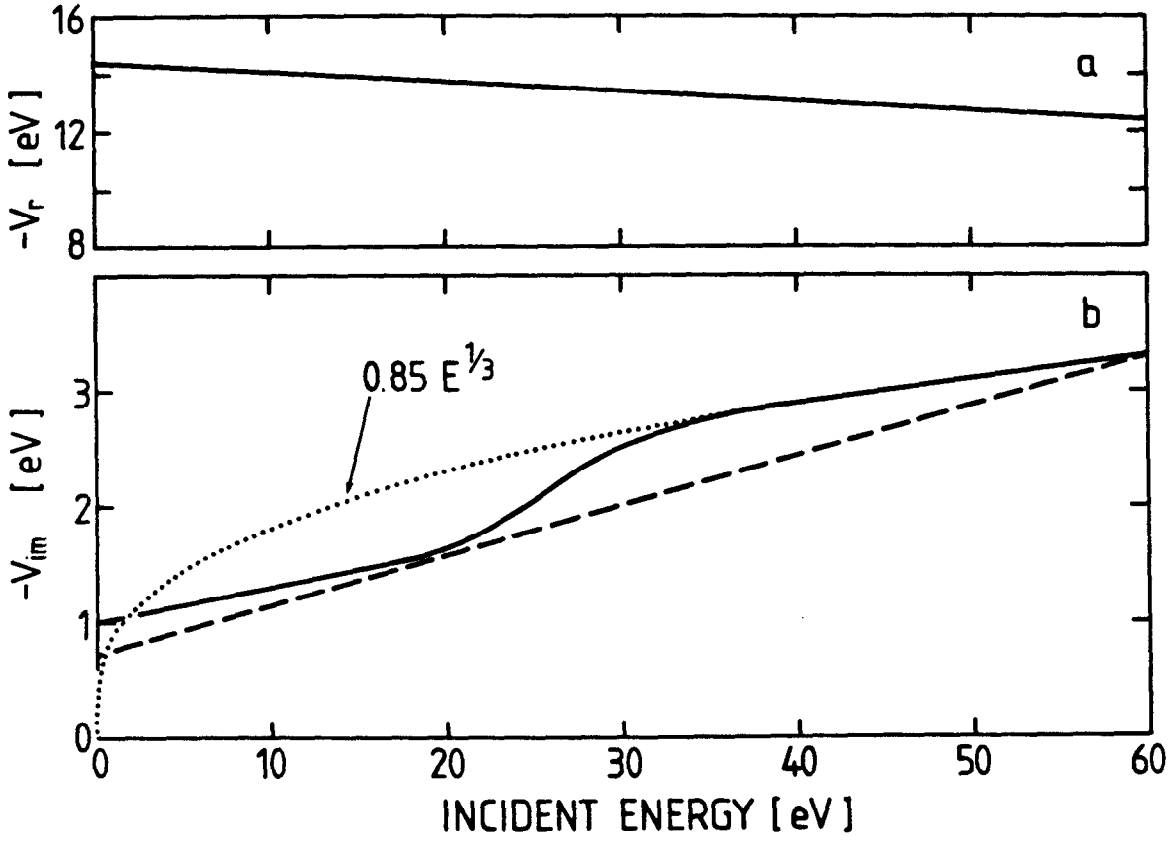
16
12
8
-Vr [eV]
a
b
0.85 E^1/3
3
2
1
0
-Vim [eV]
0
10
20
30
40
50
60
INCIDENT ENERGY [eV]

Fig. 3

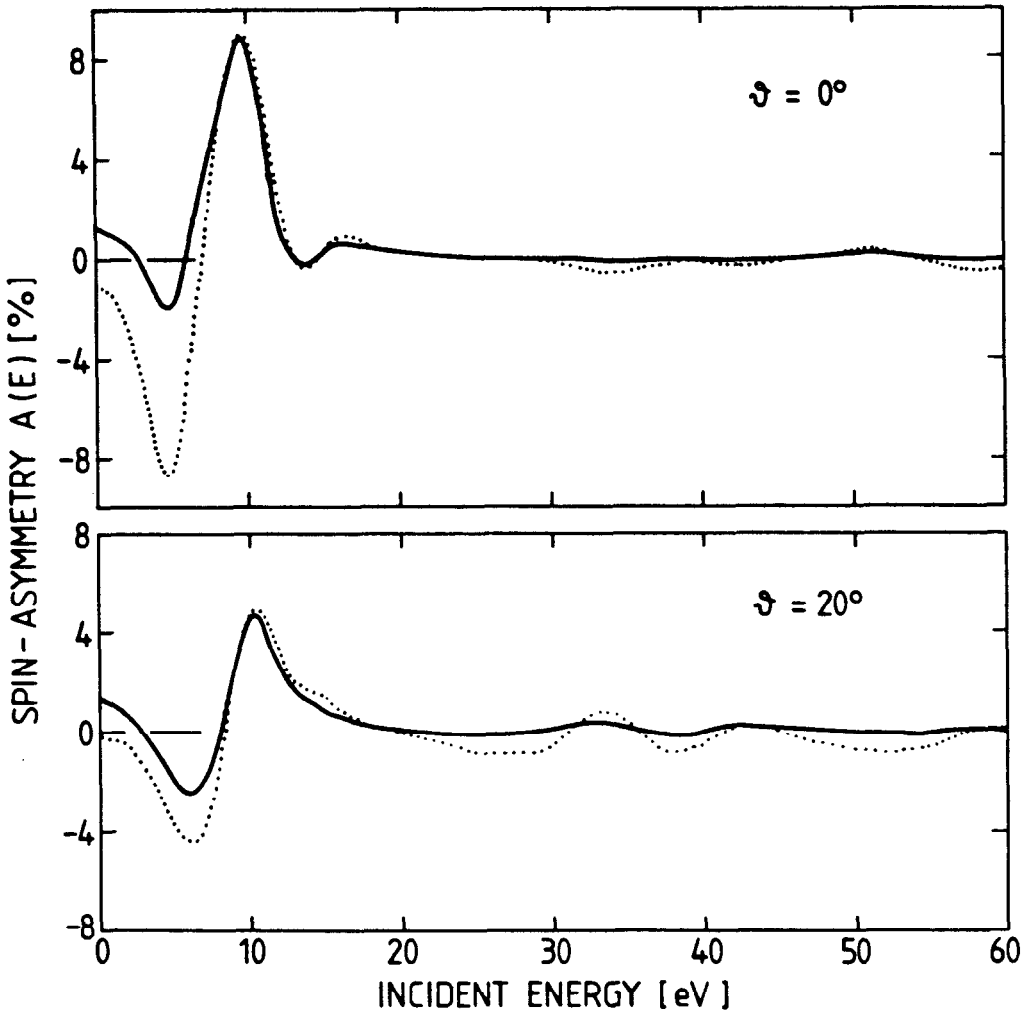
ϑ = 0°
ϑ = 20°
SPIN-ASYMMETRY A(E) [%]
INCIDENT ENERGY [eV]
8
4
0
-4
-8
0
10
20
30
40
50
60

Fig. 4